Mineralogical Magazine, December 2017, Vol. 81(6), pp. 1303–1322

Polloneite, a new complex Pb(-Ag)-As-Sb sulfosalt from the Pollone mine, Apuan Alps, Tuscany, Italy

Dan Topa[1,*], Frank N. Keutsch[2], Emil Makovicky[3], Uwe Kolitsch[1] and Werner Paar[4]

[1] Naturhistorisches Museum, Burgring 7, A-1010 Wien, Austria
[2] Harvard John A. Paulson School of Engineering and Applied Sciences and Department of Chemistry and Chemical Biology, Harvard University, 12 Oxford Street, Cambridge, MA 02138, USA
[3] Department of Geoscience and Resource Management, University of Copenhagen, Copenhagen, Østervoldgade 10, DK-1350, Copenhagen, Denmark
[4] Pezoltgasse 46, A-5020 Salzburg, Austria

[*Received 21 July 2015; Accepted 5 December 2016; Associate Editor: Allan Pring*]

ABSTRACT

Polloneite, ideally $AgPb_{46}As_{26}Sb_{23}S_{120}$, is a new $N = 4$ member of the sartorite homologous series. It occurs in a matrix of baryte from the Pizzone level of the Pollone baryte-pyrite-(Pb-Zn-Ag) deposit at Valdicastello Carducci, near Pietrasanta, in the Apuan Alps, Tuscany, Italy, as anhedral grains up to 0.5 mm across. The mineral is opaque, greyish black with a metallic lustre. In reflected light polloneite is white, bireflectance is moderate. Internal reflections are absent. Under crossed polars, anisotropism is moderate with rotation tints in brown-violet and deep grey. The reflectance data (%, air) are: 30.2, 42.4 at 470 nm, 28.8, 41.0 at 546 nm, 27.9, 39.8 at 589 nm and 26.0, 37.4 at 650 nm. Mohs hardness is 3–3½, microhardness VHN_{50} exhibits a mean value of 200 kg mm^{-2}. The average results of 15 electron-microprobe analyses of three grains are Ag 0.71(5), Pb 52.05(21), As 10.61(22), Sb 15.40(12), S 21.16(8), total 99.92(15) wt.%, corresponding to $Ag_{1.20}Pb_{45.76}As_{25.79}Sb_{23.04}S_{120.21}$ (on the basis of $Me + S = 216$ apfu). The simplified formula $AgPb_{46}As_{26}Sb_{23}S_{120}$ is in accordance with the results of a crystal structure determination. The calculated density is 5.77 g cm^{-3}. Polloneite is monoclinic, space group $P2_1$, $a =$ 8.413(2), $b = 25.901(5)$, $c = 23.818(5)$ Å, $\beta = 90.01(3)°$, $V = 5189.8(18)$ Å^3, $Z = 1$. The strongest eight lines in the calculated powder-diffraction pattern [*d* in Å(*I*)*hkl*] are 3.795(100)(026), 3.414(60)(233), 3.238(69)(080), 3.020(97)(253), 2.922(82)(066), 2.738(73)(236), 2.375(79)(290) and 2.103(64)(400). Polloneite is a new $N = 4$ member of the sartorite homologous series with substantial Sb and small, but important, Ag content. It is a three-fold superstructure with a tripled unit-cell parameter, 7.9 Å, of sartorite homologues. In the As-Sb rich slabs, several types of crankshaft chains and isolated (As,Sb)–S polyhedra occur. A sequence of three different, tightly bonded double-layer fragments (broad ribbons) contains two asymmetric fragments with long crankshaft chains whereas the third fragment type, with Ag, contains small mirror-symmetrical metalloid groups and no crankshaft chains. This configuration can potentially cause order-disorder phenomena in the structure. The threefold superstructure and the mixed As-Sb character distinguish polloneite from veenite and from dufrénoysite, respectively.

Keywords: polloneite, Pb(-Ag)-As-Sb sulfosalt, new mineral, crystal structure, sartorite homologous series, Pollone deposit, Apuan Alps, Tuscany, Italy.

Introduction

The sartorite homologous series (Makovicky, 1985), originally defined for lead-arsenic sulfosalts, now comprises at least 20 minerals. It is a combinatorial series (Makovicky, 1997), in which

*E-mail: dan.topa@nhm-wien.ac.at
https://doi.org/10.1180/minmag.2017.081.003

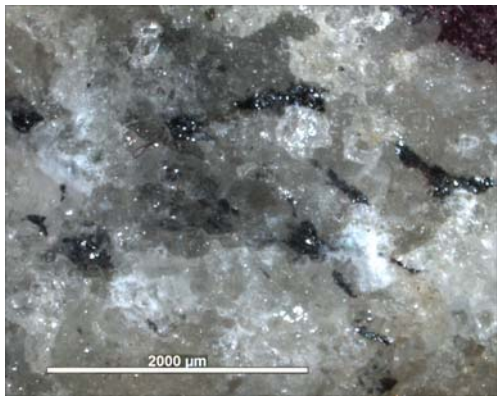

FIG. 1. Polloneite crystals enclosed in baryte.

only two pure homologues, $N = 3$ and $N = 4$, are known and the variety is created by combinations of these two unit homologue slabs in different ratios. Jambor (1967*a*,*b*) initiated the study of As-Sb sulfosalt members of this series on material from Madoc, Ontario. The Madoc samples, together with the discoveries of further As-Sb associations in Europe and Asia (e.g. Mantienne, 1974; Bracci *et al*,. 1980; Moëlo *et al.*, 1983; Lattanzi *et al.*, 1994; Johan and Mantienne, 2000; Ciobanu *et al.*, 2005; Khodaparast *et al.*, 2010), yielded enough material for the description and structural study of the As-Sb members of the sartorite homologous series – veenite (Jambor, 1967*a*,*b*; Jambor *et al.*, 1982), pierrotite (Engel *et al.*, 1983), guettardite (Makovicky *et al.*, 2012), twinnite (Makovicky and Topa, 2012), barikaite (Topa *et al.*, 2013; Makovicky and Topa, 2013), boscardinite (Orlandi *et al.*, 2012), bernarlottiite (Orlandi *et al.*, 2014) and carducciite (Biagioni *et al.*, 2014).

The Pollone baryte-pyrite-(Pb-Zn-Ag) deposit at Valdicastello Carducci, near Pietrasanta, in the Apuan Alps, Tuscany, Italy, described by Benvenuti *et al.* (1990) and Costagliola *et al.* (1998) is a well-known locality for As-Sb sulfosalts. It is the type locality for parasterryite (Moëlo *et al.*, 2011), carducciite (Biagioni *et al.*, 2014) and meerschautite (Biagioni *et al.*, 2013); sterryite and members of the geocronite/jordanite series. In addition, ferdowsiite, arsenic-bearing zinkenite and andorite have been identified there (D.T., unpublished results). A number of other Sb-sulfosalts have also been described, including boulangerite, bournonite, diaphorite (Frizzo and Simone, 1995), meneghinite and owyheeite (Carmignani *et al.*, 1976). Our study on new material from the Pollone mine extends this list of sulfosalts with yet another sulfosalt mineral. Polloneite, ideally $AgPb_{46}As_{26}Sb_{23}S_{120}$, is a new mixed As-Sb member of the sartorite homologous series, an $N = 4$ sulfosalt with a novel superstructure involving a tripled unit-cell parameter of the sartorite homologues. Together with the recently defined mineral bernarlottiite (Orlandi *et al.*, 2014), the crystal structure of polloneite heralds a new superstructure trend among the As-Sb members of the sartorite series. It is a superstructure formation by a stacking of diagonal As,Sb-rich double-layer fragments of different kinds, leading to a tripling of the typical, fundamental 7.9 Å parameter. Previously known homologues have superstructures either by stacking of different slabs along the *b* direction (e.g. baumhauerite; Engel and Nowacki, 1969) or along the 8.4 Å direction (e.g. sartorite,

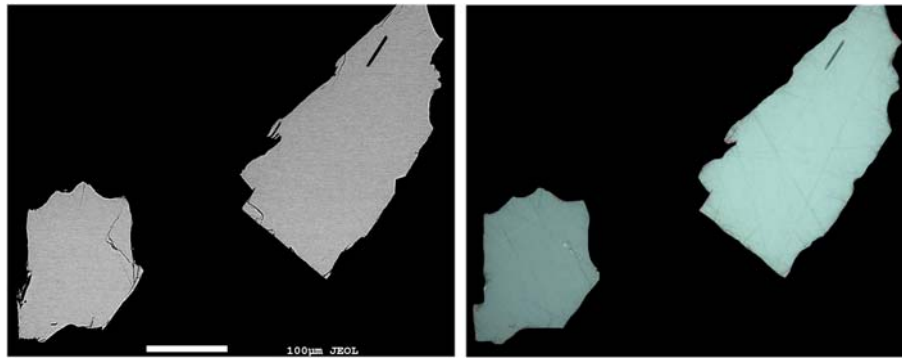

FIG. 2. High contrast, back-scattered electron (BSE) (*left*) and reflected optical (crossed-polars) (*right*) images of polloneite, confirming its homogeneity.

TABLE 1. Reflectance values (WTiC standard in air) for polloneite.

λ (nm)	R_{min}	R_{max}	λ (nm)	R_{min}	R_{max}
400	33.1	49.2	560	28.6	40.9
420	31.3	44.0	580	28.1	40.1
440	30.7	43.2	**589**	**27.9**	**39.8**
460	30.3	42.9	600	27.6	39.4
470	**30.2**	**42.4**	620	27.1	38.7
480	30.1	42.1	640	26.3	37.9
500	29.6	41.6	**650**	**26.0**	**37.4**
520	29.2	41.4	660	25.7	36.9
540	29.0	41.0	680	25.1	35.8
546	**28.8**	**41.0**	700	24.5	35.1

The reference wavelengths required by the Commission on Ore Mineralogy (COM) are given in bold.

Berlepsch *et al.*, 2003). The ordered structure of polloneite differs from the structures of dufrénoysite, $Pb_{16}As_{16}S_{40}$ (Ribar *et al.*, 1969) and veenite, $Pb_{16}Sb_{10}As_6S_{40}$ (Topa and Makovicky, 2017), which preserve the fundamental 7.9 Å periodicity. The mineral and its name have been approved by IMA-CNMNC, number 2014-093 (Topa *et al.*, 2015). The holotype specimen of polloneite is deposited in the mineralogical collection of the Naturhistorisches Museum, Vienna, Austria, catalogue number N 9786. The name is for the Pollone mine where the mineral was discovered.

Occurrence and mineral description

The mineral was found in samples collected by one of the authors (FNK) at the sterryite/parasterryite occurrence in the Pollone mine (Moëlo *et al.*, 2011) as rare crystals up to ~0.5 mm long and 0.3 mm wide in a baryte matrix (Fig. 1). The Pollone deposit is situated at the southern tip of the metamorphic complex of the Apuan Alps. Host rocks consist of a siliciclastic formation which underwent *syn*-kinematic greenschist metamorphism in the Tertiary period at ~350°C and 0.35 GPa. They are characterized by the presence of chlorite, tourmaline and, locally, arsenopyrite. According to Costagliola *et al.* (1998), fluid circulation was concentrated along shear zones, leading to vein-like baryte-pyrite-Pb-Zn-Ag sulfide mineralization, together with regional silicification and changes in Rb and Sr regimes. Mineralizing fluids were hotter than the country rock (up to 450°C) and they probably equilibrated with siliciclastic rocks and

TABLE 2. Chemical data from electron microprobe analysis of polloneite.

No.	Mean values	NA*	Ag	Pb	As	Sb	S	Total	ch#	Σ*Me*	N_{chem} §	Ag_{subs} §
1	group 1	14	0.62(10)	52.58(30)	10.45(15)	15.29(16)	21.04(13)	99.97(20)	–0.3	95.96	4.05	8.4
2	group 2	15	0.71(5)	52.05(21)	10.61(22)	15.40(12)	21.16(8)	99.92(15)	–0.6	95.79	4.02	9.9
3	group 3	13	0.85(3)	51.30(19)	10.48(11)	16.33(15)	21.08(11)	100.04(14)	0.8	96.34	3.98	12.0

The data are expressed in wt.%. *Number of analyses. #Charge balance as (Σ(val+)–Σ(val–)). §$N_{chemical}$ and Ag_{subst} are described in the text. Formulae are calculated on the basis of Σ(*Me* + S) = 216 apfu.
1: $Ag_{1.04}Pb_{46.43}(As_{25.52}Sb_{22.97})_{\Sigma=48.49}S_{120.04}$
2: $Ag_{1.20}Pb_{45.76}(As_{25.79}Sb_{23.04})_{\Sigma=48.83}S_{120.21}$
3: $Ag_{1.43}Pb_{45.06}(As_{25.45}Sb_{24.41})_{\Sigma=49.86}S_{119.66}$

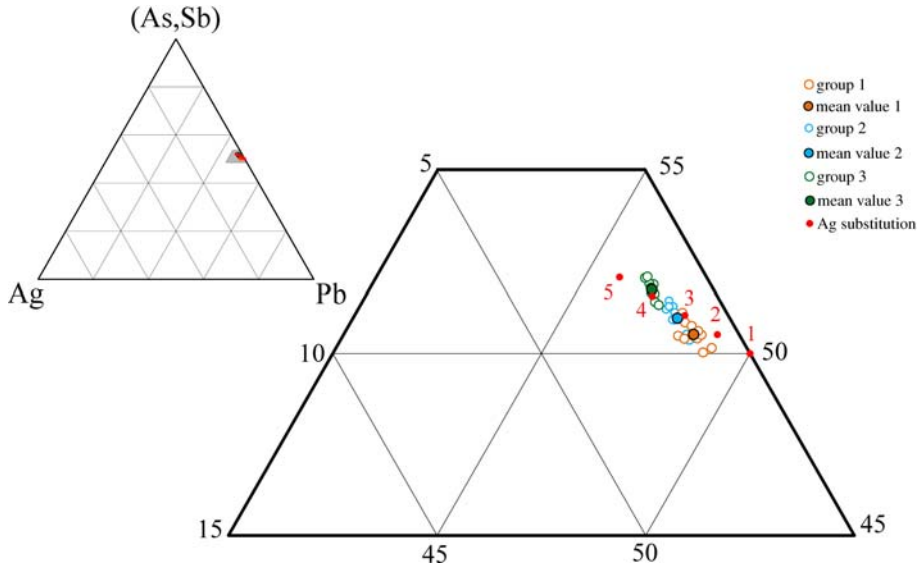

FIG. 3. Ternary Pb–(As,Sb)–Ag plot with empirical cation ratios of polloneite, their three partial averages and selected theoretical values [1: $Pb_{48}(As,Sb)_{\Sigma=48}S_{120}$, 2: $Ag_{0.5}Pb_{47}(As,Sb)_{\Sigma=48.4}S_{120}$, 3: $AgPb_{46}(As,Sb)_{\Sigma=49}S_{120}$ (corresponding to the ideal formula of polloneite), 4: $Ag_{1.5}Pb_{45}(As,Sb)_{\Sigma=49.5}S_{120}$, 5: $Ag_2Pb_{44}(As,Sb)_{\Sigma=50}S_{120}$]. The large diagram is just a small portion of the entire diagram (shown upper left).

sedimentary baryte-pyrite deposits at deeper levels. Changes in temperature, possibly connected with the tectonic events, might have been the agent causing precipitation. Besides the Pollone deposit, the Sant' Anna tectonic window, which exposes this metamorphic complex, contains the deposits of Monte Arsiccio and Buca dell'Angina, both with sulfide and sulfosalt mineralization (Lattanzi *et al.*, 1994).

Polloneite occurs as rare prismatic crystals up to 0.5 mm in size, with complex morphology but without visually observable twinning (Fig. 1). No intergrowth with sterryite or parasterryite was observed. Colour of the mineral in hand specimen is grey-black, streak is black. Polloneite is opaque, with metallic lustre. In reflected light (Fig. 2), polloneite is white, with moderate bireflectance, and no visible pleochroism. Reflectance values were obtained in air, with a WTiC standard (Table 1). They show a uniform decrease in reflectivity values from the short wavelengths to the red end of the spectrum. Internal reflections are absent, anisotropism is moderate in brown-violet and deep grey. Mohs hardness is 3–3½, derived from indentation measurements which yielded a VHN_{50} range 185–211, with the mean equal to 200 kg mm^{-2}. The mineral is brittle, without cleavage or parting, and with conchoidal fracture. Density could not be measured because of paucity of available material; $D_{(calc.)} = 5.77$ g cm^{-3} using the empirical formula.

Chemical data

Several grains of polloneite were embedded in epoxy, polished, carbon-coated and analysed using a JEOL Hyperprobe JXA-8530F electron microprobe at the Naturhistorisches Museum, Vienna, Austria. Measurements were performed at 25 kV and 20 nA, with a beam diameter of 2 µm. Wavelength dispersive spectroscopy data were collected using the following standards and emission lines: galena (Pb*Mα*), bismuthinite (Bi*Lα*), chalcopyrite (Cu*Kα*, Fe*Kα*), Ag metal (Ag*Lα*), stibnite (Sb*Lα*), cinnabar (Hg*Lα*) and lorandite (Tl*Lα*, As*Lα*, S*Kα*). The raw data were corrected for matrix effects with the JEOL on-line *ZAF* procedure. Although, randomly, Cu, Fe, Tl, Hg and Bi are present at their respective limits of detectability (0.03 for Cu and Fe and 0.15 for Tl, Hg and Bi; in wt.%), those elements are not taken into account for the mean values and empirical formulae of the three grains with different Ag contents compiled in Table 2. The empirical formula (based on 96 *Me* + 120 S apfu) of polloneite and analytical

point average #2, calculated in agreement with the results of the crystal-structure determination, is $Ag_{1.20}Pb_{45.76}$ $As_{25.79}Sb_{23.04}S_{120.21}$ (Table 2). The simplified formula, $AgPb_{46}As_{26}Sb_{23}S_{120}$, is derived from a three-fold superstructure of the dufrénoysite formula, $3 \times (Pb_{18}As_{18}S_{40})$, by partial substitution of Sb for As as well as [Ag + (As,Sb)] for 2Pb. The difference between the empirical and simplified formulas is discussed later.

The homologue order, N_{chem}, calculated for polloneite from the results of the chemical analysis (#2) according to the procedure given by Makovicky (1985) and Makovicky and Topa (2015), is 4.02, close to the ideal structural value of 4 for the 4th term of the sartorite homologous series (Fig. 3). With the calculated N value, the formula, calculated according to the general composition is $Me_{8N}S_{8N+8}$, is $Ag_{0.40}Pb_{15.37}As_{8.66}Sb_{7.74}S_{40.38}$ ($Z = 3$). This formula is based on $8N$ cations and the recalculation coefficient derived for cations was also applied to sulfur. This is the formula to be used for calculation of unbiased substitution percentages (Makovicky and Topa, 2015).

The chemical composition of polloneite indicates 9.9 mol.% of the hypothetical fully Ag-(As, Sb) substituted end-member $Ag_4Pb_8(As,Sb)_{20}S_{40}$ for analysis #2, the remaining 90 mol.% being the Ag-free end-member, the range being from 8.4 to 12.0 substitution. This separates polloneite both from the ideally Ag-free veenite region of the phase diagram, and from the compositional interval of barikaite with a pronounced (~87 mol.%) substitution of Pb by Ag + (Sb,As).

Crystallography and crystal structure

Methods

A diffractometer with an area detector system was used to perform the single-crystal study. Unit-cell parameters were refined from single-crystal data. A fragment with irregular shape 0.04 mm × 0.06 mm × 0.09 mm in size was mounted on a Bruker AXS three-circle diffractometer equipped with a CCD area detector. The *SMART* (Bruker AXS, 1998*a*) system of programs was used for unit-cell determination and data collection (*SAINT* + ; Bruker AXS, 1998*b*) for reduction of intensity data, and *XPREP* (Bruker AXS, 1997) for space-group determination and empirical absorption correction based on pseudo ψ-scans. The non-centrosymmetric space group $P2_1$ proposed by the *XPREP* program for polloneite was chosen. It is consistent with the monoclinic symmetry of the

TABLE 3. Crystal data and summary of parameters describing data collection and refinement for polloneite.

Crystal data	
Chemical formula	$Ag_{1.2}Pb_{46}As_{25}Sb_{23}S_{120}$
Unit-cell parameters	
a (Å)	8.413(2)
b (Å)	25.901(5)
c (Å)	23.817(5)
β (°)	90.01(3)
V (Å^3)	5189.8(18)
Z	1
Crystal colour	grey metallic
Crystal habit	irregular
Formula weight	8983.7
Crystal system	monoclinic
Space group	$P2_1$ (no. 4)
D_x (mg m^{-3})	5.77
No. of reflections for cell params.	4957
μ (mm^{-1})	43.8
Crystal form	irregular
Crystal size (mm)	0.11 × 0.08 × 0.05
Data collection	
T_{min}, T_{max}	0.119, 0.477
No. of measured refl.	45,627
No. of independent refl.	14,951
No. of observed refl.	9818
Criterion for observed reflections	$I > 2\sigma(I)$
R_{int} (%), $R_{(sigma)}$(%)	11.65, 10.03
θ_{max}(°)	23.3
Range of *h, k, l*	$-9 =< h =< 9$, $-28 =< k =< 28$, $-26 =< l =< 26$
Refinement	
Refinement on	F_o^2
$R[F_o > 4\sigma(F_o)]$ (%)	4.73
$wR(F_o^2)$ (%)	7.96
S (Goof)	0.872
No. of reflections used in refinement	9818
No. of parameters refined	691
$(\Delta/\sigma)_{max}$	0.02
$\Delta\rho_{max}$ (*e*/Å^3)	1.64 (0.97 Å from Pb9)
$\Delta\rho_{min}$ (*e*/Å^3)	–2.05 (0.94 Å from Pb14)
Extinction coefficient	0.000018(2)
Source of atomic scattering factors	*International Tables for X-Ray Crystallography* (Wilson, 1992, Vol. C, Tables 4.2.6.8 and 6.1.1.4)

Weighting scheme: $w = 1/[\sigma^2(F_o^2) + (aP)^2 + bP]$ where $P = (F_o^2 + 2F_c^2)/3$, a = 0.0221, b = 0

TABLE 4A. Calculated powder X-ray diffraction data for polloneite.*

$I_{rel.}$	d/Å	h k l	$I_{rel.}$	d/Å	h k l	$I_{rel.}$	d/Å	h k l
25	7.59	0 1 3	29	2.8166	2 6 3	3	1.9279	2 10 6
11	6.77	0 2 3	**73**	**2.7382**	**$\bar{2}$ 3 6**	15	1.9163	$\bar{2}$ 7 9
4	6.03	1 3 0	3	2.7056	0 9 3	17	1.9161	2 7 9
15	5.84	0 3 3	4	2.6370	$\bar{2}$ 4 6	5	1.8962	0 12 6
2	5.27	$\bar{1}$ 2 3	4	2.6366	2 4 6	14	1.8666	$\bar{2}$ 12 3
19	5.02	0 4 3	9	2.6326	0 1 9	13	1.8665	2 12 3
2	5.02	$\bar{1}$ 4 1	4	2.6307	$\bar{3}$ 1 3	5	1.8501	0 14 0
3	4.41	1 5 0	9	2.5928	0 2 9	7	1.8422	$\bar{2}$ 8 9
27	4.34	0 5 3	9	2.4624	0 10 3	6	1.8420	2 8 9
2	4.34	$\bar{1}$ 5 1	4	2.4497	0 4 9	9	1.8398	$\bar{4}$ 2 6
6	4.32	0 6 0	**79**	**2.3752**	**2 9 0**	10	1.8395	4 2 6
53	4.15	2 1 0	14	2.3300	0 9 6	6	1.8394	$\bar{4}$ 6 3
2	4.09	$\bar{1}$ 1 5	2	2.2760	2 7 6	7	1.8393	4 6 3
8	3.970	0 0 6	7	2.2756	$\bar{2}$ 9 3	20	1.8248	$\bar{2}$ 11 6
21	3.924	0 1 6	7	2.2755	2 9 3	20	1.8246	2 11 6
2	3.856	1 5 3	6	2.2574	0 11 3	3	1.8168	4 3 6
4	3.841	1 6 0	14	2.2561	0 6 9	18	1.8018	0 14 3
100	**3.795**	**0 2 6**	37	2.2318	$\bar{2}$ 1 9	3	1.8006	2 13 0
73	3.792	0 6 3	41	2.2314	2 1 9	3	1.7908	$\bar{2}$ 1 12
2	3.782	2 3 0	11	2.1692	0 10 6	4	1.7906	2 1 12
18	3.607	0 3 6	3	2.1683	$\bar{2}$ 3 9	6	1.7807	0 13 6
3	3.590	1 0 6	4	2.1680	2 3 9	9	1.7781	$\bar{2}$ 2 12
32	3.573	$\bar{2}$ 2 3	2	2.1549	$\bar{2}$ 8 6	8	1.7779	2 2 12
36	3.572	2 2 3	2	2.1547	2 8 6	3	1.7677	$\bar{2}$ 9 9
58	3.414	$\bar{2}$ 3 3	12	2.1525	0 7 9	3	1.7676	2 9 9
60	3.414	2 3 3	11	2.1251	$\bar{2}$ 10 3	17	1.7638	4 8 0
4	3.384	0 4 6	12	2.1250	2 10 3	6	1.7494	$\bar{4}$ 5 6
3	3.354	0 7 3	**64**	**2.1033**	**4 0 0**	6	1.7492	4 5 6
2	3.315	$\bar{1}$ 3 6	3	2.0828	0 12 3	3	1.7218	$\bar{4}$ 8 3
12	3.265	2 5 0	2	2.0682	4 2 1	3	1.7217	4 8 3
69	**3.238**	**0 8 0**	2	2.0561	$\bar{2}$ 5 9	9	1.7071	$\bar{4}$ 6 6
45	3.224	$\bar{2}$ 4 3	2	2.0558	2 5 9	10	1.7069	4 6 6
44	3.223	2 4 3	6	2.0546	2 11 0	3	1.6962	$\bar{2}$ 5 12
56	3.151	0 5 6	24	2.0490	0 8 9	4	1.6959	2 5 12
86	3.020	$\bar{2}$ 5 3	2	2.0381	2 9 6	4	1.6873	0 15 3
87	**3.020**	**2 5 3**	3	1.9883	$\bar{2}$ 6 9	2	1.6609	$\bar{4}$ 7 6
26	2.9979	0 8 3	3	1.9881	2 6 9	2	1.6607	4 7 6
82	**2.9220**	**0 6 6**	2	1.9848	0 0 12	5	1.6575	$\bar{2}$ 6 12
13	2.8873	$\bar{2}$ 0 6	6	1.9618	0 2 12	5	1.6573	2 6 12
10	2.8868	2 0 6	12	1.9480	0 9 9	2	1.5760	0 2 15
4	2.8695	$\bar{2}$ 1 6	2	1.9398	$\bar{4}$ 4 3	3	1.5754	0 10 12
4	2.8690	2 1 6	3	1.9397	4 4 3	9	1.5616	0 3 15
17	2.8181	$\bar{2}$ 2 6	20	1.9343	0 3 12	3	1.5613	$\bar{4}$ 9 6
15	2.8176	2 2 6	4	1.9325	0 13 3	10	1.5421	0 4 15
23	2.8168	$\bar{2}$ 6 3	3	1.9280	$\bar{2}$ 10 6	3	1.5386	$\bar{4}$ 6 9

*The theoretical pattern was calculated with *PowderCell 2.3* software (Kraus and Nolze, 1999) in Debye-Scherrer configuration employing Cu$K\alpha$ radiation ($\lambda = 1.540598$ Å), a fixed slit, and no anomalous dispersion, for $I_{rel} > 1.99$. Unit-cell parameters, space group, atom positions, site occupancy factors and isotropic displacement factors from the crystal-structure determination were used. The strongest lines are given in bold.

lattice and intensity statistics. The structure of polloneite was solved by direct methods (*SHELXS-97*; Sheldrick, 2008), which revealed most of the atom positions. In subsequent cycles of the refinement (Sheldrick, 2008), remaining atom positions were deduced from difference-Fourier

TABLE 4B. Experimental powder X-ray diffraction data for polloneite.

d/Å	$I_{est.}$*	$I_{calc.}$ from Table 4*a*
3.80	m	173
3.42	w	118
3.24	m	148
3.02	s	281
2.40	w	93
2.13	w	87

*s = very strong; m = medium; w = weak

syntheses by selecting from among the strongest maxima at appropriate distances. The final agreement factors are $R_1 = 0.047$ for 9818 reflections with $Fo > 4\sigma(Fo)$ and 0.079 for all 14,951 data. The crystal measured showed a combination of racemic twinning and, not unexpected from the pseudo-orthorhombic metrics of the unit cell, twinning by pseudo-merohedry (twin law $\bar{1}00/0\bar{1}0/001$), in good agreement with the order-disorder (OD) character of the structure described below. The refined pseudo-merohedric twin ratio was 0.434:0.076; the refined inversion twin ratio was also 0.434:0.076, thus indicating that each pseudo-merohedric twin component shows ideal inversion twinning. Experimental powder X-ray diffraction data were derived from measurements of a single-crystal specimen on an Oxford Diffraction Xcalibur E diffractometer, using graphite-monochromatized Mo*K*α radiation (λ = 0.71073 Å) at ambient temperature and integrating the results as a simulated powder diffraction pattern. The experimental data obtained had broad peaks (full width at half maximum (FWHM) ≈ 0.15) but showed good consistency with the intensities and *d* spacings calculated using *Jade9* (v9.5.0, MDI Materials Data, California, USA, 2012) software on the basis of the structural model (see below); only calculated reflections with $I > 2$ are reported (if not observed). The β value close to 90°, and the relative closeness of the large *b* and *c* parameters, cause a substantial crowding of reflections in the powder X-ray diffraction data, expressed at large FWHM values. Observed intensities were estimated visually.

Structure data

Polloneite is monoclinic, space group $P2_1$, $a = 8.413(2)$, $b = 25.901(5)$, $c = 23.818(5)$ Å, $\beta = 90.01(3)°$, $V = 5189.8(18)$ Å^3, $Z = 1$. The *a*:*b*:*c* ratio calculated from the single-crystal unit cell parameters is 0.325:1:0.920. Complete experimental and refinement data for polloneite are collected in Table 3. Calculated and experimental powder diffraction data are given in Tables 4*a* and 4*b*. Atom position parameters, refined occupancies and U_{eq} parameters are listed in Table 5; a crystallographic information file (cif) of complete anisotropic displacement parameters has been deposited with the Principal Editor of *Mineralogical Magazine* at http://www.minersoc.org/pages/e_journals/dep_mat_mm.html and is also available upon request from the authors. Bond distances are presented in Table 6 and polyhedron characteristics in Table 7.

The unit cell of polloneite is a supercell of the fundamental motif of the sartorite homologous series for the homologue $N = 4$. Unit-cell parameters are $a = 8.4133(6)$, $b = 25.901(2)$, $c = 23.818(2)$ Å and $\beta = 90.011(1)°$. The *c* parameter represents a triple of the typical 7.94 Å (in this Pb-rich case) value whereas the *a* and *b* parameters are typical for $N = 4$ homologues (e.g. dufrénoysite and rathite). The β value corresponds to those of dufrénoysite and veenite (Jambor, 1967*a*,*b*) but is different from that of rathite (100.7°, Table 8). If site occupancy differences between consecutive structure portions along [001] are disregarded, the overall picture in the [100] projection (Figs 4 and 5) resembles that of projected dufrénoysite ($N = 4$). It has zig-zag walls of tricapped trigonal coordination prisms of Pb and intervening slabs, in which As, Sb and Pb combine in a scheme generally conforming to the SnS archetype with lone electron pairs situated between tightly bonded double layers which are populated by cations and anions (Fig. 4). At first sight, bernarlottiite, $P\bar{1}$, with $a = 23.501$, $b = 8.386$, $c = 23.704$ Å, $\alpha = 89.88$, $\beta = 102.93$, $\gamma = 89.91°$ (Orlandi *et al.*, 2014) appears metrically close to polloneite, but it is an $N_{1,2} = 3;4$ homologue and its crystal structure is a three-fold superstructure of baumhauerite, which is triclinic, $a = 7.884(4)$, $b = 8.345(4)$, $c = 22.811(11)$ Å, $\alpha = 90.069(8)$, $\beta = 97.255(8)$, $\gamma = 90.082(8)°$, $V = 1488.8(13)$ Å^3, space group $P1$ (lattice data for $Pb_{11.80}As_{16.28}S_{35.92}$ from Moosegg, Austria; Topa and Makovicky, 2016).

The structure of polloneite contains 48 distinct metal and 60 sulfur sites. There are 33 fully occupied cation sites (18 Pb, 6 Sb, 9 As) and 15 mixed sites (Table 5). The Ag site, Me15, apparently contains at least 30–40% Sb and the set of observed *Me*–S distances is similar to that of the Me10 site, which has longer distances but otherwise fully corresponds to the configuration of

TABLE 5. Coordinates, occupancy factors and displacement parameters of atoms in polloneite.

Site	Atom	Occupancy	*x*/*a*	*y*/*b*	*z*/*c*	$U_{ani/iso}$
Pb1	Pb	1	0.3775(5)	0.17275(16)	0.15745(17)	0.0410(10)
Pb2	Pb	1	0.8763(4)	0.16537(13)	0.15422(16)	0.0321(9)
Pb3	Pb	1	0.3856(4)	0.26364(14)	0.31946(16)	0.0402(10)
Pb4	Pb	1	0.8885(4)	0.26618(13)	0.32846(15)	0.0343(9)
Pb5	Pb	1	0.3650(4)	0.16957(15)	0.49147(17)	0.0428(11)
Pb6	Pb	1	0.8735(4)	0.17399(15)	0.48950(15)	0.0351(10)
Pb7	Pb	1	0.3773(4)	0.26487(15)	0.65783(16)	0.0364(10)
Pb8	Pb	1	0.8759(5)	0.27170(14)	0.65545(17)	0.0383(10)
Pb9	Pb	1	0.3874(4)	0.17277(14)	0.81851(15)	0.0366(9)
Pb10	Pb	1	0.8896(5)	0.17095(14)	0.82801(16)	0.0397(10)
Pb11	Pb	1	0.3651(4)	0.26775(15)	0.99252(17)	0.0431(11)
Pb12	Pb	1	0.8750(4)	0.26334(14)	0.98992(15)	0.0317(9)
Pb13	Pb	1	0.3775(4)	0.39414(13)	0.10521(14)	0.0245(8)
Pb14	Pb	1	0.6228(4)	0.54377(14)	0.39512(14)	0.0294(9)
Pb15	Pb	1	0.8894(4)	0.3984(2)	0.4303(2)	0.0296(9)
Pb16	Pb	1	0.6371(4)	0.54380(14)	0.72991(15)	0.0337(9)
Pb17	Pb	1	0.3621(4)	0.39301(13)	0.77021(14)	0.0245(8)
Pb18	Pb	1	0.6270(4)	0.53952(15)	0.06607(16)	0.0357(10)
Sb1	Sb	1	0.8813(7)	0.4089(2)	0.0951(2)	0.0289(15)
Sb2	Sb	1	0.1189(6)	0.5273(2)	0.4036(2)	0.0194(13)
Sb3	Sb	1	0.4196(6)	0.5213(2)	0.5414(2)	0.0209(13)
Sb4	Sb	1	0.8698(7)	0.5221(2)	0.5453(3)	0.0393(17)
Sb5	Sb	1	0.1336(6)	0.5312(2)	0.7364(2)	0.0174(13)
Sb6	Sb	1	0.5771(7)	0.4173(2)	0.9592(2)	0.0232(14)
As1	As	1	0.8708(9)	0.6335(3)	0.3144(3)	0.021(2)
As2	As	1	0.1277(9)	0.3051(3)	0.1849(3)	0.019(2)
As3	As	1	0.3775(9)	0.6317(3)	0.6474(3)	0.0193(19)
As4	As	1	0.9344(9)	0.6208(3)	0.6546(3)	0.0172(19)
As5	As	1	0.1233(9)	0.3104(3)	0.5082(4)	0.021(2)
As6	As	1	0.6231(8)	0.4092(3)	0.6194(3)	0.0097(16)
As7	As	1	0.8729(9)	0.6278(3)	0.9895(3)	0.022(2)
As8	As	1	0.0651(8)	0.3171(3)	0.8463(3)	0.0187(19)
As9	As	1	0.6213(9)	0.3061(3)	0.8523(3)	0.0186(19)
Me1	Pb/Sb	0.61(1)/0.39(1)	0.3733(4)	0.39780(14)	0.43428(16)	0.0185(9)
Me2	Pb/Sb	0.66(2)/0.34(2)	0.8694(5)	0.51810(18)	0.87710(19)	0.0378(15)
Me3	Pb/Sb	0.79(1)/0.21(1)	0.1097(4)	0.53925(14)	0.06961(15)	0.0224(9)
Me4	Sb/As	0.55(4)/0.45(4)	0.3795(7)	0.5289(3)	0.2109(2)	0.026(2)
Me5	Sb/Pb	0.50(2)/0.50(2)	0.8494(5)	0.51614(17)	0.21558(18)	0.0367(16)
Me6	Sb/Pb	0.71(2)/0.29(2)	0.1523(5)	0.42259(18)	0.28376(18)	0.0254(15)
Me7	Sb/Pb	0.50(2)/0.50(2)	0.1320(5)	0.41999(18)	0.62179(19)	0.0318(15)
Me8	Sb/Pb	0.55(1)/0.45(1)	0.8642(6)	0.4059(2)	0.7635(2)	0.0475(18)
Me9	Sb/As	0.70(2)/0.30(2)	0.3754(8)	0.5272(3)	0.8794(3)	0.040(2)
Me10	mixed	–	0.3827(8)	0.6267(2)	0.9864(3)	0.0325(18)
Me11	As/Sb	0.75(4)/0.25(4)	0.3215(9)	0.6242(3)	0.3216(3)	0.021(2)
Me12	As/Sb	0.76(4)/0.24(4)	0.6787(9)	0.3144(3)	0.1776(3)	0.026(3)
Me13	As/Sb	0.73(4)/0.27(4)	0.6205(8)	0.4079(3)	0.2895(3)	0.021(2)
Me14	As/Sb	0.76(2)/0.24(4)	0.1305(7)	0.4154(2)	0.9540(3)	0.0111(15)
Me15	mixed	–	0.6161(8)	0.3113(2)	0.5133(3)	0.0270(17)
S1	S	1	0.116(2)	0.3593(7)	0.0319(7)	0.018(4)
S2	S	1	0.609(2)	0.3469(6)	0.0279(7)	0.014(4)
S3	S	1	0.101(2)	0.4582(7)	0.1455(7)	0.022(5)
S4	S	1	0.653(2)	0.4653(7)	0.1518(8)	0.026(5)
S5	S	1	0.166(2)	0.5763(7)	0.2573(8)	0.029(5)
S6	S	1	0.597(2)	0.5694(6)	0.2564(7)	0.021(4)

(continued)

TABLE 5. (*contd*.)

Site	Atom	Occupancy	*x*/*a*	*y*/*b*	*z*/*c*	$U_{ani/iso}$
S7	S	1	0.090(2)	0.6590(6)	0.3675(7)	0.015(4)
S8	S	1	0.669(2)	0.6560(7)	0.3720(8)	0.018(4)
S9	S	1	0.385(2)	0.7342(6)	0.4310(7)	0.017(4)
S10	S	1	0.878(2)	0.7495(6)	0.4239(6)	0.019(4)
S11	S	1	0.120(2)	0.1929(6)	0.0705(7)	0.021(4)
S12	S	1	0.629(2)	0.2040(7)	0.0709(8)	0.030(5)
S13	S	1	0.324(2)	0.2850(7)	0.1288(8)	0.017(4)
S14	S	1	0.913(2)	0.2841(6)	0.1293(7)	0.024(5)
S15	S	1	0.416(2)	0.3660(7)	0.2445(7)	0.022(4)
S16	S	1	0.831(2)	0.3663(6)	0.2391(7)	0.016(4)
S17	S	1	0.359(2)	0.4717(7)	0.3495(7)	0.019(4)
S18	S	1	0.905(2)	0.4765(7)	0.3524(8)	0.023(5)
S19	S	1	0.382(2)	0.5880(7)	0.4717(8)	0.031(5)
S20	S	1	0.875(2)	0.5801(7)	0.4660(8)	0.023(5)
S21	S	1	0.373(2)	0.7029(7)	0.5898(8)	0.026(5)
S22	S	1	0.888(2)	0.6935(7)	0.6029(8)	0.025(5)
S23	S	1	0.135(2)	0.2382(6)	0.2429(8)	0.020(5)
S24	S	1	0.632(2)	0.2447(7)	0.2334(8)	0.025(5)
S25	S	1	0.118(2)	0.3533(6)	0.3592(8)	0.015(4)
S26	S	1	0.628(2)	0.3505(6)	0.3662(6)	0.020(4)
S27	S	1	0.147(2)	0.4647(6)	0.4823(7)	0.025(4)
S28	S	1	0.601(2)	0.4658(6)	0.4835(7)	0.018(4)
S29	S	1	0.085(2)	0.5743(7)	0.5920(8)	0.024(5)
S30	S	1	0.653(2)	0.5687(7)	0.5913(7)	0.023(5)
S31	S	1	0.161(2)	0.6552(6)	0.7022(7)	0.010(4)
S32	S	1	0.577(2)	0.6576(7)	0.7037(8)	0.020(4)
S33	S	1	0.338(2)	0.2843(6)	0.4583(7)	0.034(5)
S34	S	1	0.907(2)	0.2822(7)	0.4593(8)	0.021(5)
S35	S	1	0.419(2)	0.3606(6)	0.5784(7)	0.020(4)
S36	S	1	0.825(2)	0.3635(7)	0.5750(8)	0.022(5)
S37	S	1	0.352(3)	0.4738(8)	0.6872(9)	0.026(5)
S38	S	1	0.894(2)	0.4697(7)	0.6822(8)	0.026(5)
S39	S	1	0.367(2)	0.5782(5)	0.7992(5)	0.016(4)
S40	S	1	0.866(2)	0.5922(7)	0.8028(8)	0.020(5)
S41	S	1	0.129(2)	0.3494(7)	0.6969(8)	0.023(5)
S42	S	1	0.612(2)	0.3558(5)	0.6984(6)	0.018(4)
S43	S	1	0.100(2)	0.4659(7)	0.8173(8)	0.020(5)
S44	S	1	0.654(2)	0.4643(8)	0.8143(9)	0.022(5)
S45	S	1	0.168(2)	0.5753(7)	0.9242(8)	0.022(5)
S46	S	1	0.585(2)	0.5749(7)	0.9254(7)	0.025(5)
S47	S	1	0.129(2)	0.2042(6)	0.7423(8)	0.020(5)
S48	S	1	0.642(2)	0.1951(6)	0.7325(7)	0.015(4)
S49	S	1	0.428(2)	0.2846(6)	0.7951(7)	0.016(4)
S50	S	1	0.842(2)	0.2865(8)	0.7970(9)	0.033(5)
S51	S	1	0.341(2)	0.3673(7)	0.9122(7)	0.020(4)
S52	S	1	0.917(2)	0.3680(7)	0.9070(8)	0.021(5)
S53	S	1	0.390(2)	0.4696(6)	0.0145(7)	0.021(5)
S54	S	1	0.861(2)	0.4680(5)	0.0153(6)	0.016(4)
S55	S	1	0.123(2)	0.0883(7)	0.8588(9)	0.026(5)
S56	S	1	0.636(2)	0.0826(6)	0.8681(7)	0.023(4)
S57	S	1	0.110(2)	0.2486(7)	0.8984(8)	0.020(5)
S58	S	1	0.622(2)	0.2399(6)	0.9107(8)	0.016(4)
S59	S	1	0.331(2)	0.1617(5)	0.9591(6)	0.010(3)
S60	S	1	0.909(2)	0.1550(7)	0.9617(7)	0.017(4)

TABLE 6. Selected interatomic distances (Å) in polloneite.

Pb1–		Pb2–		Pb3–		Pb4–		Pb5–		Pb6–	
S13	3.020(19)	S11	2.947(17)	S32	2.819(19)	S31	2.994(16)	S21	3.058(18)	S21	2.903(18)
S11	3.042(17)	S45	3.012(19)	S23	2.864(18)	S23	2.997(18)	S33	3.084(16)	S34	2.907(19)
S12	3.063(18)	S12	3.044(18)	S24	2.956(18)	S25	3.059(17)	S19	3.125(18)	S22	3.021(18)
S40	3.074(18)	S40	3.056(18)	S15	3.206(18)	S22	3.123(18)	S22	3.157(18)	S19	3.230(18)
S46	3.227(18)	S14	3.147(16)	S26	3.231(16)	S34	3.148(19)	S20	3.236(18)	S29	3.249(19)
S23	3.344(18)	S39	3.242(13)	S21	3.357(18)	S24	3.177(18)	S9	3.262(17)	S9	3.277(17)
S32	3.352(19)	S31	3.444(17)	S25	3.370(17)	S26	3.225(16)	S30	3.276(18)	S20	3.393(18)
S24	3.366(18)	S24	3.465(18)	S33	3.374(17)	S21	3.364(18)	S8	3.283(19)	S7	3.441(17)
S39	3.420(13)	S23	3.571(18)	S22	3.467(18)	S16	3.389(16)	S10	3.539(16)	S10	3.529(16)
Pb7–		Pb8–		Pb9–		Pb10–		Pb11–		Pb12–	
S10	2.925(16)	S10	2.863(16)	S47	2.947(18)	S47	2.994(18)	S59	2.875(14)	S60	2.900(18)
S8	2.934(19)	S7	2.984(16)	S49	2.969(16)	S55	2.996(18)	S58	2.998(18)	S58	2.908(18)
S9	3.019(17)	S36	3.084(19)	S48	3.020(17)	S50	3.109(21)	S2	3.022(16)	S57	2.968(18)
S35	3.138(16)	S41	3.092(18)	S6	3.220(16)	S48	3.147(17)	S57	3.143(18)	S12	3.220(18)
S41	3.166(18)	S9	3.161(17)	S55	3.264(18)	S57	3.208(18)	S51	3.217(18)	S2	3.241(16)
S42	3.222(13)	S42	3.274(14)	S56	3.350(16)	S60	3.215(17)	S13	3.295(19)	S11	3.355(16)
S47	3.299(18)	S48	3.343(17)	S59	3.395(15)	S5	3.218(19)	S1	3.301(18)	S1	3.360(18)
S49	3.336(17)	S50	3.405(22)	S58	3.426(18)	S56	3.272(16)	S12	3.338(18)	S52	3.373(19)
S48	3.374(17)	S47	3.445(18)	S57	3.595(18)	S58	3.484(18)	S11	3.386(17)	S14	3.378(17)
Pb13–		Pb14–		Pb15–		Pb16–		Pb17–		Pb18–	
S53	2.915(17)	S20	2.870(18)	S18	2.749(19)	S40	2.880(18)	S41	2.858(18)	S4	2.813(19)
S13	2.917(18)	S28	2.923(17)	S25	2.816(18)	S44	2.881(21)	S42	2.877(14)	S56	2.932(17)
S2	2.948(17)	S19	2.957(18)	S26	2.954(15)	S39	2.949(13)	S37	2.880(21)	S53	2.960(17)
S1	2.950(17)	S8	2.984(19)	S27	3.032(16)	S32	3.055(19)	S49	2.923(16)	S54	2.961(14)
S3	3.014(18)	S17	3.097(18)	S34	3.091(19)	S38	3.106(18)	S43	3.112(18)	S55	3.037(19)
S4	3.162(18)	S18	3.116(18)	S28	3.249(16)	S37	3.174(24)	S44	3.247(19)	S59	3.241(14)
S15	3.412(17)	S6	3.377(17)	S36	3.603(19)	S30	3.366(17)	S51	3.451(17)	S46	3.491(17)
Sb1–		Sb2–		Sb3–		Sb4–		Sb5–		Sb6–	
S54	2.446(15)	S27	2.490(17)	S19	2.417(19)	S20	2.414(20)	S43	2.579(19)	S53	2.459(17)
S3	2.547(18)	S18	2.541(18)	S28	2.508(17)	S30	2.446(18)	S37	2.638(24)	S2	2.465(17)
S4	2.765(19)	S17	2.796(18)	S30	2.603(18)	S29	2.518(19)	S39	2.750(13)	S51	2.622(18)
S1	2.796(18)	S20	2.879(18)	S27	3.062(17)	S28	3.069(17)	S38	2.875(18)	S54	3.035(15)
S2	3.222(17)	S19	3.162(18)	S29	3.356(18)	S27	3.149(17)	S40	3.173(18)	S52	3.370(18)
S14	3.344(16)	S7	3.526(16)	S37	3.728(22)	S38	3.538(20)	S31	3.321(16)	S44	3.716(22)

As1–		As2–		As3–		As4–		As5–		As6–	
S8	2.259(19)	S13	2.187(19)	S32	2.250(19)	S22	2.283(20)	S10	2.259(17)	S36	2.325(19)
S47	2.275(18)	S23	2.217(19)	S21	2.299(20)	S29	2.298(20)	S33	2.262(18)	S42	2.337(16)
S7	2.332(18)	S14	2.305(18)	S31	2.325(18)	S31	2.387(18)	S34	2.280(19)	S35	2.342(18)
S6	3.155(18)	S15	3.219(18)	S30	3.134(19)	S30	3.114(19)	S35	3.267(19)	S38	3.144(19)
S5	3.196(19)	S16	3.225(18)	S29	3.163(19)	S32	3.364(19)	S36	3.274(19)	S37	3.257(24)
As7–		As8–		As9–		Me1–		Me2–		Me3–	
S11	2.211(18)	S57	2.198(20)	S49	2.193(18)	S17	2.785(18)	S40	2.611(19)	S3	2.771(18)
S59	2.280(15)	S52	2.320(20)	S58	2.208(19)	S27	2.815(16)	S44	2.732(20)	S56	2.836(16)
S60	2.283(19)	S50	2.351(20)	S50	2.333(20)	S28	2.852(16)	S43	2.761(18)	S55	2.891(19)
S46	3.174(19)	S51	3.089(18)	S51	3.180(19)	S26	2.950(15)	S46	3.035(18)	S54	3.075(14)
S45	3.230(19)	S49	3.394(18)	S52	3.233(19)	S33	3.010(16)	S45	3.125(18)	S60	3.093(18)
						S25	3.023(18)	S54	3.539(15)	S53	3.246(17)
						S35	3.586(17)			S45	3.620(19)
Me4–		Me5–		Me6–		Me7–		Me8–		Me9–	
S56	2.343(17)	S55	2.586(20)	S25	2.556(18)	S41	2.558(19)	S38	2.558(19)	S39	2.324(14)
S6	2.374(17)	S4	2.602(18)	S17	2.663(18)	S38	2.782(18)	S44	2.623(20)	S45	2.395(19)
S5	2.440(19)	S6	2.710(17)	S15	2.815(17)	S37	2.792(23)	S43	2.827(18)	S46	2.416(19)
S4	3.161(19)	S3	3.085(18)	S18	2.992(18)	S35	3.044(17)	S42	2.930(14)	S43	3.174(19)
S3	3.357(18)	S5	3.242(18)	S16	3.249(17)	S36	3.171(18)	S41	3.102(18)	S44	3.249(20)
S17	3.622(18)	S18	3.448(19)	S3	3.447(17)	S27	3.521(17)	S50	3.199(21)	S53	3.549(18)
Me10–		Me11–		Me12–		Me13–		Me14–		Me15–	
S12	2.425(19)	S48	2.264(18)	S24	2.276(20)	S15	2.302(18)	S1	2.360(18)	S9	2.397(17)
S46	2.609(18)	S5	2.365(20)	S16	2.366(18)	S26	2.356(17)	S51	2.383(18)	S35	2.605(18)
S45	2.689(19)	S7	2.408(17)	S14	2.414(18)	S16	2.397(18)	S52	2.447(19)	S36	2.660(19)
S60	2.844(18)	S6	3.133(18)	S15	3.038(18)	S17	3.101(19)	S53	2.969(18)	S33	2.774(17)
S59	2.886(15)	S8	3.266(19)	S13	3.292(19)	S18	3.336(19)	S54	3.022(15)	S34	2.866(19)
S56	3.652(18)					S4	3.611(20)			S26	3.649(16)

TABLE 7. Polyhedron characteristics for cation sites in polloneite.

Site	1*	2	3	4	5	6	7	8
Pb1	9	3.206	0.0146	0.1901	0.9163	138.071	66.575	1.635
Pb2	9	3.196	0.0137	0.2847	0.9170	136.723	65.983	1.737
Pb3	9	3.170	0.0087	0.2850	0.8860	133.454	64.729	1.987
Pb4	9	3.162	0.0159	0.1571	0.9041	132.432	63.772	1.823
Pb5	9	3.220	0.0185	0.1574	0.9056	139.805	67.141	1.545
Pb6	9	3.211	0.0192	0.2824	0.9146	138.692	66.563	1.760
Pb7	9	3.150	0.0113	0.2132	0.9318	130.983	63.369	1.914
Pb8	9	3.171	0.0111	0.2400	0.9067	133.613	64.653	1.844
Pb9	9	3.228	0.0129	0.2571	0.8828	140.861	68.035	1.624
Pb10	9	3.177	0.0151	0.1972	0.9254	134.320	64.734	1.742
Pb11	9	3.170	0.0117	0.1817	0.8837	133.458	64.538	1.847
Pb12	9	3.184	0.0207	0.2551	0.9142	135.158	64.763	1.850
Pb13	7	3.058	0.0762	0.2249	0.9100	119.793	41.879	1.998
Pb14	7	3.076	0.0717	0.3705	0.9327	121.863	42.806	2.120
Pb15	7	3.057	0.0760	0.2270	0.9405	119.611	41.820	1.980
Pb16	7	3.065	0.0736	0.2459	0.9711	120.594	42.274	1.932
Pb17	9	3.151	0.0504	0.3793	0.8071	131.017	60.874	2.232
Pb18	7	3.067	0.0794	0.2979	0.9217	120.802	42.084	2.008
Sb1	6	2.882	0.1136	0.4734	0.9677	100.314	28.302	2.813
Sb2	6	2.934	0.1229	0.4993	0.9621	105.801	29.540	2.586
Sb3	6	2.987	0.1217	0.6109	0.9546	111.642	31.211	2.919
Sb4	6	2.985	0.1650	0.6285	0.9008	111.440	29.620	3.337
Sb5	6	2.924	0.1256	0.4100	0.9655	104.728	29.149	2.306
Sb6	6	2.977	0.1258	0.5937	0.9482	110.488	30.747	2.886
As1	5	2.754	0.2984	0.6339	0.9992	87.513	12.695	2.955
As2	5	2.764	0.3100	0.6913	0.9729	88.404	12.611	3.375
As3	5	2.740	0.2856	0.6191	0.9968	86.141	12.724	2.948
As4	5	2.851	0.4394	0.6560	0.9916	97.072	11.251	2.702
As5	5	2.862	0.4129	0.7249	0.9891	98.152	11.915	3.075
As6	5	2.987	0.1818	0.7035	0.8982	96.663	11.181	2.641
As7	5	2.820	0.4041	0.6841	0.9687	93.979	11.579	3.186
As8	5	2.847	0.4428	0.6898	0.9988	96.652	11.135	2.968
As9	5	2.754	0.3055	0.6836	0.9864	87.538	12.569	3.326
Me1	6	3.008	0.0803	0.3032	0.8206	114.055	39.696	2.428
Me2	6	3.008	0.0943	0.4317	0.9707	113.962	32.855	2.575
Me3	7	3.079	0.0784	0.3731	0.9164	122.285	42.644	2.090
Me4	6	3.019	0.1613	0.7070	0.8980	115.262	30.771	3.865
Me5	6	2.989	0.1211	0.4624	0.9889	111.838	31.287	2.215
Me6	6	2.998	0.1377	0.4340	0.9789	112.922	30.995	2.100
Me7	6	3.025	0.1127	0.4280	0.9695	116.003	32.764	1.950
Me8	6	2.890	0.1045	0.3446	0.9628	101.103	28.819	2.311
Me9	6	2.998	0.1698	0.6915	0.9302	112.894	29.833	3.970
Me10	6	2.890	0.1760	0.5379	0.8830	101.151	26.530	2.936
Me11	5	2.839	0.4303	0.6228	0.9693	95.836	11.287	2.573
Me12	5	2.818	0.4086	0.6220	0.9869	93.698	11.456	2.552
Me13	5	2.982	0.1611	0.7054	0.8559	91.048	11.252	2.538
Me14	5	2.770	0.3966	0.5203	0.9994	89.050	11.109	2.358
Me15	6	2.866	0.2020	0.5494	0.8649	98.623	25.051	1.404

*1: coordination number; 2: radius r_s in Å of a circumscribed sphere, least-squares fitted to the coordination polyhedron; 3: volume distortion $\upsilon = [V(\text{ideal polyhedron}) - V(\text{real polyhedron})]/V(\text{ideal polyhedron})$, the ideal polyhedron has the same number of ligands; 4: 'volume-based' eccentricity $ECC_V = 1-[(r_s-\Delta)/r_s]^3$, Δ is the distance between the centre of the sphere and the central atom in the polyhedron; 5: 'volume-based' sphericity $SPH_V = 1-3\sigma_r r_s$, σ_r is a standard deviation of the radius r_s; 6: volume in Å^3 of the circumscribed sphere; 7: volume in Å^3 of coordination polyhedron; 8: bond-valence sum. All values were calculated with *IVTON* program (Balić Žunić and Vicković 1996).

TABLE 8. Comparative data for polloneite and related sartorite homologues with $N = 4$.

Mineral	Polloneite	Dufrénoysite	Rathite	Carducciite	Barikaite[#]	Veenite
Formula	$AgPb_{46}As_{26}Sb_{23}S_{120}$	$Pb_{16}As_{16}S_{40}$	$Ag_2Pb_{9.5}Tl_{1.5}As_{18}SbS_{40}$	$Ag_2Pb_{12}As_{10}Sb_8S_{40}$	$Ag_3Pb_{10}As_{11}Sb_8S_{40}$	$Pb_{16}Sb_{10}As_6S_{40}$
Crystal system	monoclinic	monoclinic	monoclinic	monoclinic	monoclinic	orthorhombic
Space group	$P2_1$	$P2_1$	$P2_1/c$	$P2_1/c$	$P2_1/c$	?
Cell parameters (Å)						
a	8.413(2)	8.47(4)	8.496(1)	8.4909(3)	8.53	8.44
b	25.901(5)	25.74(4)	7.969(1)	8.0227(3)	8.08	26.2
c	23.817(5)	7.90(1)	25.122(3)	25.3957(9)	24.95	7.9
β(°)	90.01(3)	90.35(12)	100.704(2)	100.382(2)	100.66	
Z	1	1	1	1	1	1
Ref.*	1	2	3	4	5	6

*1: this study; 2: Ribar *et al.* (1969); 3: Berlepsch *et al.* (2002); 4: Biagioni *et al.* (2014); 5: Topa *et al.* (2013); 6: Jambor (1967*a*,*b*).
[#]Transformed from: $P2_1/n$, $a = 8.533(1)$, $b = 8.075(1)$, $c = 24.828(2)$ and $\beta = 99.077(1)$.

the Ag-bearing Me15 site. Obviously, Me10 contains a portion of Ag as well. Because of mixed (Ag,Sb) sites with close atomic number values, Ag contents cannot be derived reliably from the crystal-structure refinement. We do not consider bond-valence calculations a reliable alternative. In Table 7, the bond valence of Me10 was calculated as pure Sb whereas that of Me15 as pure Ag. Other mixed positions show problems in the bond-valence sum because they were calculated for the pure major cation; some cations have similar problems because they occur in environments determined by mixed cation sites which imply averaged sulfur positions.

With the above mentioned limitations, a structural formula of polloneite is $Pb_{21.8}As_{12.75}(Sb + Ag)_{13.45}S_{60}$. Valence calculations based on this formula and compensation of a negative valence (38.15–) left after partial valence compensation by Pb and As distributes 13.45 (Sb + Ag) as 12.35 Sb and 1.1 Ag. With 0.9 Sb mixing with Ag on two sites, the structural formula can be recast as $Pb_{21.8}(Sb,As)_{24.2}(Sb,Ag)_2S_{60}$ or $Pb_{21.8}As_7Sb_6(Sb,As)_{11.2}(Sb,Ag)_2S_{60}$. For the unit-cell contents, these values should be doubled. The difference between the structural formula and the above quoted empirical chemical formula becomes clear when inspecting Figs 1 and 3, and Table 2. Polloneite displays a restricted range of Ag substitution percentages, with different percentages present in different grains, and of the As-for-Sb substitution, and, as Fig. 1 shows, it was not possible to analyse the same tiny crystal both on a diffractometer and under the electron microprobe beam.

In general, the crystal structure of polloneite is derived from the dufrénoysite structure by the partial substitution $Ag + Sb \leftrightarrow 2Pb$, connected with local cation rearrangements. Each of the Sb1, Sb2 and Sb5 sites shows flipping behaviour, and the refinement averaged two close Sb positions. This results in two opposing 2.8–2.9 Å bonds while the remaining bonds have typical Sb–S values (Table 6). For mixed sites, the lengths of the averaged interatomic distances agree well with their mixed character (As–Sb and Sb–Pb, respectively). As6 has slightly longer bonds than the rest of the As–S coordination polyhedra.

Structure modules

Columns of tricapped trigonal coordination prisms of Pb form two subsets, those with a larger volume V_S (137–141 Å^3) and those of smaller volume

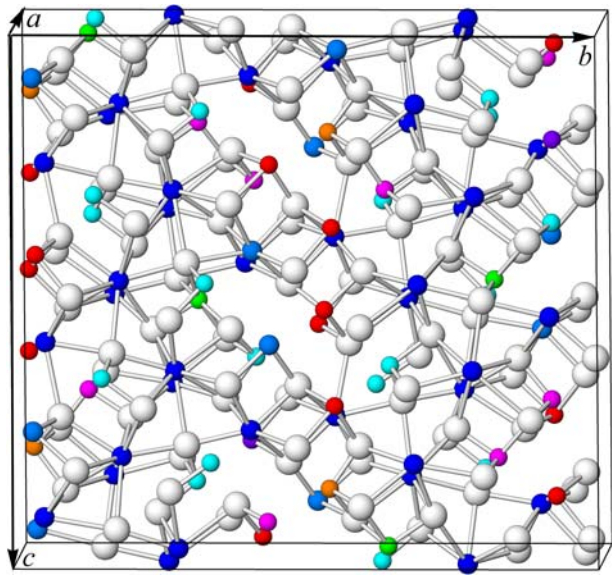

FIG. 4. The crystal structure of polloneite projected along [100]. S spheres are white, Pb are dark blue, As are cyan, Sb are red; the mixed (presumed) (Pb,Sb) sites are bright blue, the (Sb,Pb) sites dark violet, the (Sb,As) sites orange, the (As, Sb) sites bright violet and the (Sb,Ag) sites green. The *c* axis is vertical.

(131–134 Å^3) (Table 7). These alternate in the structure. They alternate also at the two ends of a tightly bonded ribbon, e.g. Pb1,2 and Pb7,8 columns at the ends of the ribbon type which will be named R2 below. There is no obvious correlation of these V_S values with the values of cation eccentricity, or of the polyhedron sphericity, or those of distortion (Table 7). In general, a column with the larger prisms is surrounded by coordination polyhedra with a larger degree of Pb-for-Sb and Sb-for-As substitution than that with smaller prisms, but the picture is far from simple, especially at the contact of two R3 ribbons which contain Me3 sites. The seven-fold coordination prisms of Pb in the body of the As-Sb double layers have uniform V_S volumes of ~120 ± 1 Å^3. Large volumes of the trigonal prisms centred by Pb1, Pb5 and Pb9 result in excessively low bond-valence sums.

Of the three-member [001] sequence of tightly bonded fragments of double layers in the SnS-like slabs (Fig. 6), two adjacent fragments of double layers, which will be called the 'R1 layers' and 'R3 layers' or such 'ribbons' according to typical cation sites Me1 and Me3 which they contain, respectively (Figs 7 and 8), are similar and approximately inversion related to one another. There are (As,Sb)–S crankshaft chain fragments, formed by four and, when Me1 is Sb, five (As,Sb)–S polyhedra, respectively, on the opposing surfaces of a double layer of this kind. Chains on opposing surfaces of an R1 or of an R3 double layer are perpendicular to one another and always combine As and Sb. The crank-shaft chains on those surfaces of the R1 and R3 double-layer pair, which face one another *via* a common interlayer volume, are parallel and are related by approximate inversion centres.

When we examine configuration and coordination details, R1 and R3 ribbons are similar but contain some substantial differences. The sequence of cations in the outer crankshaft chain of the R1 ribbon is As3–As4–Sb4–Sb3–Me1 (Me = $Pb_{61}Sb_{39}$, expressed as occupancy percentages), accompanied by a disconnected site, Me15(Pb) (Fig. 7). The analogous crankshaft chain in the R3 ribbon is As9–As8–Me14–Sb6–Pb18 (Me = $As_{76}Sb_{24}$), whereas the off-chain site is Me3 (refined as $Pb_{79}Sb_{21}$) (Fig. 8). As mentioned above, the contact of the R1 and R3 ribbons takes place *via* imperfect inversion centres; these are situated between Me5 and Me6 sites, and between Me4 and Me13 sites. The As1 site inverts into As2 and Sb1 into Sb2. The mixed site $(As_{75}Sb_{25})$11 is projected into the site $(As_{76}Sb_{24})$12 but the remaining inversion-paired sites are disparately occupied; the site $(Sb_{55}As_{45})$4 becomes $(As_{73}Sb_{27})$13, and $(Sb_{50}As_{50})$5 becomes $(Sb_{71}As_{29})$6. The Sb1 site is a well-balanced, split

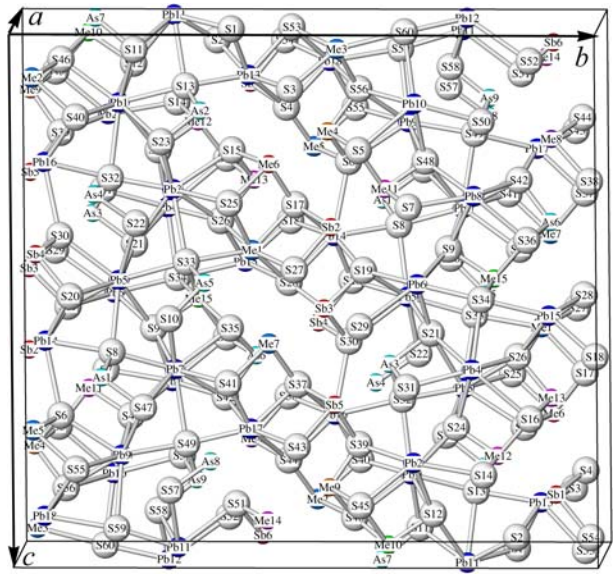

FIG. 5. Atom notation for polloneite; oblique projection on (100).

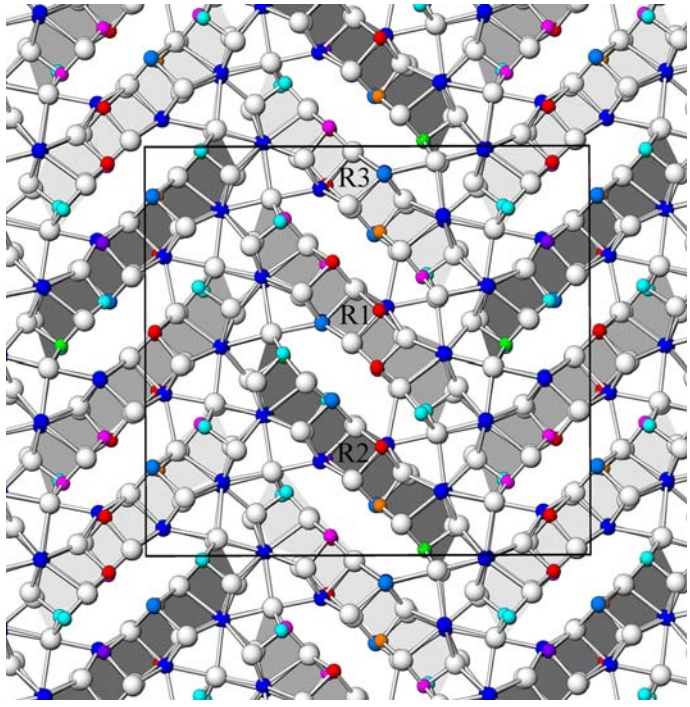

FIG. 6. Compartmentalized structure with a definition and sequence of three types of double-layer ribbons ('R1', 'R2' and 'R3' ribbons), ribbon interconnections *via* trigonal coordination prisms of Pb and inter-ribbon spaces. Orientation as in Fig. 4.

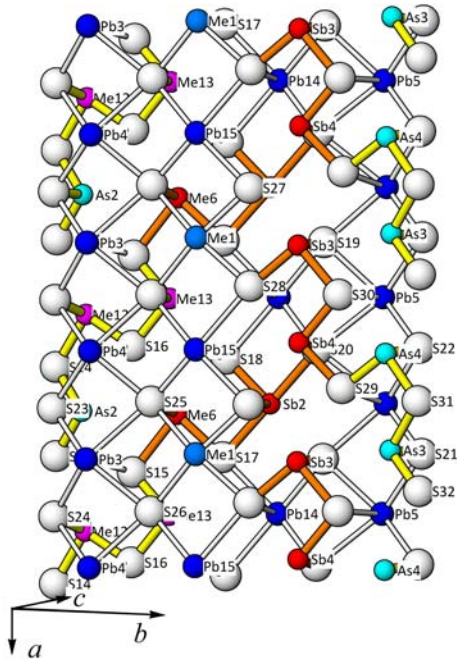

FIG. 7. The 'R1' ribbon in a slightly oblique projection. Note interconnection of crankshaft chains on the two surfaces of the double layer (defined in the text) *via* short bonds of Sb2, Sb3, Sb4 and Me1 to sulfur.

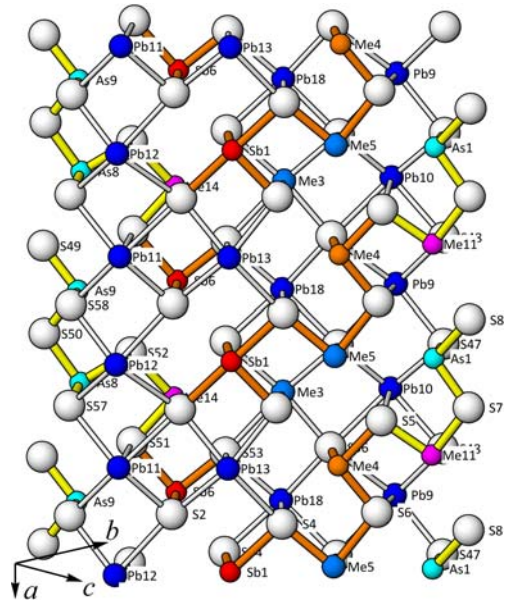

FIG. 8. The 'R3' ribbon in a slightly oblique projection. The same orientation as in Fig.7. Compare the orientation of crankshaft chains in this ribbon and in the structurally adjacent 'R1' ribbon (Fig. 7). Crankshaft chains on the two surfaces are interconnected *via* short bonds of Me14, Me3, Me4 and Me5 to sulfur. Configurational similarity to the 'R1' ribbon is visible; differences are described in the text.

flipping position whereas the analogous Sb2 site is a split position with less balanced component occupancies.

The remaining type of double layer, R2, which represents a third of all double layers, namely those which contain the Me2 site, is built differently (Fig. 9). In a close approximation, the faces of this double layer contain mirror-symmetrical (As, Sb)$_x$S$_y$ and isolated (As,Sb)S$_2$ configurations, and display marginal cation positions indicating mixed Sb-Ag sites. The identical configurations on the two faces are shifted by 2 Å in the [100] direction, and are related by imperfect inversion centres. The R2 double-layer ribbon has a detailed architecture different from R1 and R3 ribbons. Its surfaces contain Me2–S43–Me8–S44 and Sb5–S37–Me7–S38 cation pairs. Pseudosymmetry interconverts three different *Me* sites in this ribbon (all *Me* = $Sb_{50\pm5}$ $Pb_{50\pm5}$), and it treats a balanced flipping Sb5 site as one of them. Furthermore, the ribbon contains an 'isolated' Me9 site, occupied by $Sb_{70}As_{30}$, and three isolated As5, As6 and As7 sites occupied by pure As (Fig. 9). Me9 and As6 are backed by trapezoidal configurations interpreted as 'Me15' and 'Me10', respectively. Both of them are probably the mixed (Ag,Sb) sites with similar coordination.

Each surface of the R2 ribbon has a series of near perfect mirror planes parallel to (100), running through and between the Me2–Me8 pairs and, approximately through the Me7–Sb5 pairs. Together with the intralayer inversion centres this means that, e.g. when we take the Me2–Me8 surface as the initial surface, the Me7–Sb5 group can be centred either on the S43 atom of the initial surface or on the S44 atom of this surface, as a reflection of the previous configuration (compare Fig. 9). Thus, for the configurations on the second, 'derived' surface, we have a local OD freedom of 4.2 Å. The surfaces of the R2-type double-layer ribbon are very different to the surfaces of the R1 and R3 ribbons, which are formed by diagonal crankshaft chains that comprise four or five (As, Sb)–S polyhedra. The surface of the R2 ribbon is configurationally close to an individual $(100)_{PbS}$ plane in the crystal structure of ramdohrite (Makovicky and Mumme, 1983; Makovicky *et al.*, 2013). They share among themselves the

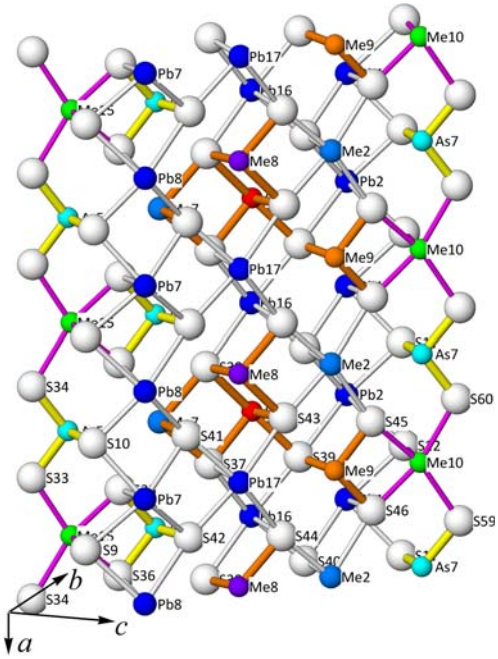

FIG. 9. The 'R2' ribbon in a slightly oblique projection. Note the pairs and individual polyhedra of metalloids on the surfaces of the double layer, interconnected by short bonds of Sb5, Me8 and Me9 to sulfur. The surfaces have mirror reflections parallel to (100) situated *via* metalloid pairs and between them; they are shifted on the opposing surface by ~2.1 Å along [100]. Flipping of the Sb5 site (red in the figure) partly violates this symmetry.

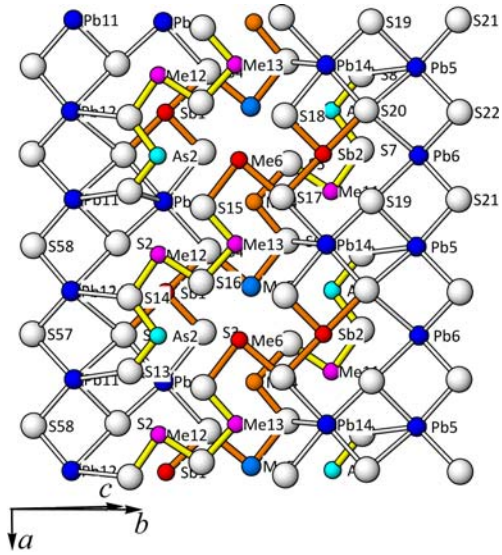

FIG. 10. The contact of the 'R1' (front) and 'R3' (back) ribbons *via* a common inter-ribbon space, illustrated by showing only the two surfaces in contact. Note the antiparallel orientation of nearly identical crankshaft chains.

trapezoidal character of coordination pyramids, and the approximate symmetries in the atomic plane. However, there are substantial differences in the orientation of some of the short cation–anion bonds.

The contact of the R1 and R3 ribbons *via* (imperfect) inversion symmetry (Fig. 10) fixes their mutual position and the antiparallel orientation of the crankshaft chains in the facing planes: As2–Me12($As_{76}Sb_{24}$)–Me13($As_{73}Sb_{27}$)–Me6($Sb_{71}As_{29}$)–Sb2 in the R1 ribbon *vs.* As1–Me11($As_{75}Sb_{25}$)–Me4($Sb_{55}As_{45}$)–Me5($Sb_{50}Pb_{50}$) – flipping Sb1 in the R3 ribbon. The same holds for the mutual position of the outer chains (both of which face the respective R2 ribbons), As3–As4–Sb4–Sb3–Me1($Pb_{61}Sb_{39}$) in the R1 ribbons and As9–As8–Me14($As_{76}Sb_{24}$) –Sb6···Pb18 in the R3 ribbons. The contact of the R3 and R2 ribbons (Fig. 11), however, leaves a free choice of two orientations, [100] and [$\bar{1}$00], for the R3 ribbon with its diagonally running crankshaft chains; the R1–R3 pair derived from this R3 ribbon should then follow the chosen orientation as a block. The R1 ribbon has cation composition $Pb_{6.9}As_{4.49}Sb_{4.61}$, i.e. As ≈ Sb, the R2 ribbon has corresponding composition $Pb_{7.61}As_{3.3}(Sb,Ag)_{5.09}$, with Sb > As, and the R3 ribbon is composed of $Pb_{7.29}As_{4.96}Sb_{3.75}$, with As > Sb; all cases with 16 cation sites. The prominent Sb > As character of the R2 ribbon determines its unique configurations and affinity to Ag. By contrast, none of the polyhedra in the R1 and R3 ribbons exhibits features suggesting substitution by Ag.

Twinning and order-disorder phenomena

We carefully studied a possible extension of the positional order-disorder predicted for the median plane of R2 ribbons, and of the orientational order-disorder on the contacts of R3 (and potentially R1) ribbons with R2 ribbons, throughout the entire structure (Fig. 6). Both operations result in shifts by a height of one prism, parallel to [100], of the columns of the alternating larger and smaller trigonal coordination prisms of Pb on both ends of the ribbon. Any propagation of disorder to adjacent ribbons will proceed *via* these prisms. We suggest that orientation reversal of an

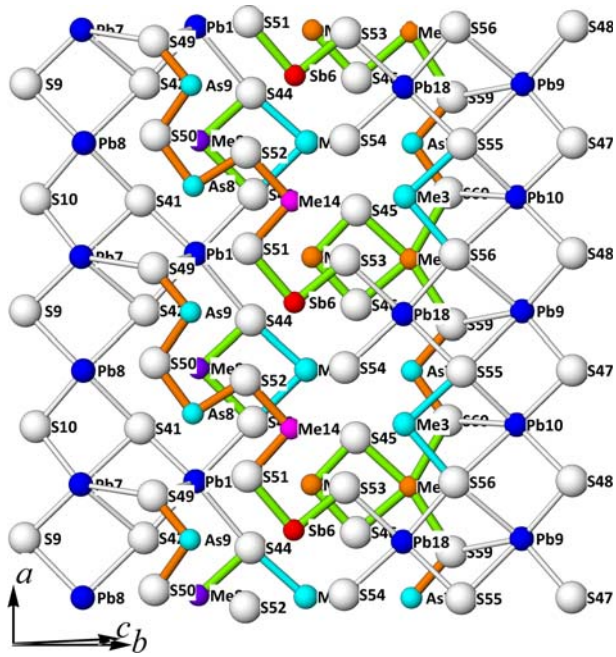

FIG. 11. The contact of the 'R2' (front) and 'R3' (back) ribbons illustrating the ambiguity of the 'R3' orientation in relation to the surface of the 'R2' double layer.

R1–R3 block after an R2 ribbon during the growth along the [001] direction will influence the position and orientation of the adjacent R2 ribbons(s) which lie to the right and to the left of the reversed R1–R3 ribbon pair (Fig. 6), and also of the R1 ribbons which immediately precede these R2 ribbons in the flanking rows. These reoriented R1 ribbons will have misfit problems with the R1–R3 match in their inversed R3–R1 pairs, and in general, the order-disorder scheme is expected to strain the Pb prism sequences. These problems, however, could hypothetically also be taken care of by the adaptable configurations of the bounding layers of trigonal Pb prisms. Thus, the presence or absence of these phenomena remains unresolved: the crystal-structure refinement (above) suggests minor twinning and orientational disorder in the crystal studied (which might influence the values of the refined mixed site occupancies) but optical data (Fig. 2) do not corroborate this suggestion.

Conclusion

The crystal structure of polloneite offers another confirmation of the importance of crystal-chemical differences between arsenic and antimony in the 3+ valence state in the crystal structures of sulfides. Partial mixing of these two cations in some structure sites should not obscure their spatial separation and creation of new structure schemes or even types, when both are present in substantial amounts, as in polloneite, barikaite, etc. When one of them predominates, the structure is determined by it and is in general different from that of the opposite cation, as illustrated by As_2S_3 and Sb_2S_3, but the central portions of intermediate regions of the As- and Sb-based binary systems have to accommodate disparate coordination requirements of both cations by creating a novel structural solution. Accommodation of Ag in a separate one third of double-layer segments, namely the R2 ribbons, surrounded by double layers without this feature, is apparently connected with higher concentrations of As and lower concentrations of Sb in the R1 and R3 layers, which also lack Ag. These combined features are two reasons for the existence of this remarkable superstructure. Its existence is connected with higher Sb contents in the ore-forming solutions than those observed, e.g. in the Lengenbach deposit, and with a moderate but definite silver-for-metalloid substitution, situated between those values of veenite and rathite.

Acknowledgements

FNK is grateful to Cristian Biagioni, who guided him to the occurrence of polloneite and helped in the collection process and without whom this work would not have been possible. Careful reviews by Yves Moëlo and Allan Pring are gratefully acknowledged.

References

Balić Žunić, T. and Vicković, I. (1996) *IVTON* – program for the calculation of geometrical aspects of crystal structures and some crystal chemical applications. *Journal of Applied Crystallography*, **29**, 305–306.

Benvenuti, M., Costagliola, P., Tanelli, G., Cortecci, G. and Lattanzi, P. (1990) Geology, mineralogy and geochemistry of the barite-pyrite (Pb-Ag) deposit at Pollone, Apuan Alps. *Bollettino della Societa Geologica Italiana*, **109**, 735–741.

Berlepsch, P., Armbruster, T. and Topa, D. (2002) Structural and chemical variations in rathite, $Pb_8Pb_{4-x}(Tl_2As_2)_x(Ag_2As_2)As_{16}S_{40}$: modulations of a parent structure. *Zeitschrift für Kristallographie*, **217**, 581–590.

Berlepsch, P., Armbruster, T., Makovicky, E. and Topa, D. (2003) Another step toward understanding the true nature of sartorite: determination and refinement of a nine-fold superstructure. *American Mineralogist*, **88**, 450–461.

Biagioni, C., Moëlo, Y., Orlandi, P., Stanley, C.J. and Evain, M. (2013) Meerschautite, IMA 2013-061. CNMNC Newsletter No. 17, October 2013, page 3004; *Mineralogical Magazine*, **77**, 2997–3005.

Biagioni, C., Orlandi, P., Moëlo, Y. and Bindi, L. (2014) Lead-antimony sulfosalts fromTuscany, (Italy). XVI. Carducciite, $(AgSb)Pb_6(As,Sb)_8S_{20}$, a new Sb-rich isotype of rathite from the Pollone mine, Valdicastello Carducci: occurrence and crystal structure. *Mineralogical Magazine*, **78**, 1775–1793.

Bracci, G., Dalena, D., Orlandi, P., Duchi, G. and Vezzalini, G. (1980) Guettardite from Tuscany, Italy: A second occurrence. *The Canadian Mineralogist*, **18**, 13–15.

Bruker AXS (1997) *SHELXTL, Version 5.1*. Bruker AXS, Inc., Madison, WI 53719,USA.

Bruker AXS (1998*a*) *SMART, Version 5.0*. Bruker AXS, Inc., Madison, WI 53719, USA.

Bruker AXS (1998*b*) *SAINT, Version 5.0*. Bruker AXS, Inc., Madison, WI 53719, USA.

Carmignani, L., Dessau, G. and Duchi, G. (1976) I giacimenti abarite, pirite ed ossidi de ferro delle Alpi Apuane. Studio minerogenetico e strutturale. Nuove osservazioni sui giacimenti polimetallici. *Bollettino della Societa Geologica Italiana*, **95**, 1009–1061.

Ciobanu, C.L., Cook, N.J., Capraru, N., Damina, G. and Cristea, P. (2005) Mineral assemblages from the vein salband at Săcărimb, Golden Quadrilateral, Romania: I. Sulphides and sulphosalts. Au-Ag-Te-Se deposits, IGCP Project 486. Bulgarian Academy of Sciences. *Geochemistry, Mineralogy and Petrology (Sofia)*, **43**, 47–55.

Costagliola, P., Benvenuti, M., Lattanzi, P. and Tanelli, G. (1998) Metamorphogenic barite-pyrite (Pb-Zn-Ag) veins at Pollone, Apuane alps, Tuscany: vein geometry, geothermobarometry, fluid inclusions and geochemistry. *Mineralogy and Petrology*, **62**, 29–60.

Engel, P. and Nowacki, W. (1969) Kristallstruktur von Baumhauerit. *Zeitschrift für Kristallographie*, **129**, 178–202.

Engel, P., Gostojic, M. and Nowacki, W. (1983) The crystal structure of pierrotite, $Tl_2(Sb,As)_{10}S_{16}$. *Zeitschrift für Kristallographie*, **165**, 209–215.

Frizzo, P. and Simone, S. (1995) Diaphorite in the Pollone ore deposit (Apuan Alps, Tuscany, Italy). *European Journal of Mineralogy*, **7**, 705–708.

Jambor, J.L. (1967*a*) New lead sulfantimonides from Madoc, Ontario – Part 1. *Canadian Mineralogist*, **9**, 7–24.

Jambor, J.L. (1967*b*) New lead sulfantimonides from Madoc, Ontario. Part 2 – Mineral descriptions. *Canadian Mineralogist*, **9**, 191–213.

Jambor, J.L., Laflamme, J.H.G. and Walker, D.A. (1982) A re-examination of the Madoc sulfosalts. *Mineralogical Record*, **13**, 93–100.

Johan, Z. and Mantienne, J. (2000) Thallium-rich mineralization at Jas Roux, Hautes-Alpes, France: a complex epithermal, sediment-hosted, ore-forming system. *Journal of the Czech Geological Society*, **45**, 63–77.

Khodaparast, M., Tajedin, H. and Shahrokhi, V. (2010) Nature of fluid inclusions of gold mineralization at Barika shear zone: Example of Kuroko type gold mineralization in the west of Iran. *The 1st International Applied Geological Congress, Islamic Azad University – Mashad Branch*, Iran, 26-28 April 2010.

Kraus, W. and Nolze, G. (1996) *POWDER CELL* – a program for the representation and manipulation of crystal structures and calculation of the resulting X-ray powder patterns. *Journal of Applied Crystallography*, **29**, 301–303.

Lattanzi, P., Benvenuti, M., Costagliola, P. and Tanelli, G. (1994) An overview on recent research on the metallogeny of Tuscany with special reference to the Apuane Alps. *Memorie della Società Geologica Italiana*, **48**, 613–625.

Makovicky, E. (1985) The building principles and classification of sulphosalts based on the SnS archetype. *Fortschritte der Mineralogie*, **63**, 45–89.

Makovicky, E. (1997) Modular crystal chemistry of sulphosalts and other complex sulphides. Pp. 237–271 in: *Modular Aspects of Minerals* (S. Merlino, editor).

European Mineralogical Union, Notes in Mineralogy, **1**. Eötvös University Press, Budapest.

Makovicky, E. and Mumme, W.G. (1983) The crystal structure of ramdohrite, $Pb_6Sb_{11}Ag_3S_{24}$, and its implications for the andorite group and zinckenite. *Neues Jahrbuch für Mineralogie, Abhandlungen*, **147**, 58–79.

Makovicky, E. and Topa, D. (2012) Twinnite, $Pb_{0.8}Tl_{0.1}Sb_{1.3}As_{0.8}S_4$, the OD character and the question of its polytypism. *Zeitschrift für Kristallographie*, **227**, 468–475.

Makovicky, E. and Topa, D. (2013) The crystal structure of barikaite. *Mineralogical Magazine*, **77**, 3093–3104.

Makovicky, E. and Topa, D. (2015) Crystal chemical formula for sartorite homologues. *Mineralogical Magazine*, **79**, 25–31.

Makovicky, E., Topa, D., Tajjedin, H., Rastad, E. and Yaghubpur, A. (2012) The crystal structure of guettardite, $PbAsSbS_4$, and the twinnite-guettardite problem. *Canadian Mineralogist*, **50**, 253–266.

Makovicky, E., Mumme, W.G. and Gable, R.W. (2013) The crystal structure of ramdohrite, $Pb_{5.9}Fe_{0.1}Mn_{0.1}In_{0.1}Cd_{0.2}Ag_{2.8}Sb_{10.8}S_{24}$: A new refinement. *American Mineralogist*, **98**, 773–779.

Mantienne, J. (1974) *La Minéralisation Metallifère de Jas-Roux (Hautes-Alpes)*. PhD Thesis, Université de Paris 6, France.

Moëlo, Y., Borodaev, Y.S. and Mozgova, N.N. (1983) Association twinnite-zinkénite-plagionite du gisement complexe à Sb–Pb–Zn de Rujevac (Yougoslavie). *Bulletin de Minéralogie*, **106**, 505–510.

Moëlo, Y., Orlandi, P., Guillot-Deudon, C., Biagioni, C., Paar, W. and Evain, M. (2011) Lead-antimony sulfosalts from Tuscany (Italy). XI. The new mineral parasterryite, $Ag_4Pb_{20}(Sb_{14.5}As_{9.5})_{\Sigma 24}S_{58}$, and associated sterryite, $Cu(Ag,Cu)_3Pb_{19}(Sb,As)_{22}(As\text{-}As)S_{56}$, from Pollone mine (Tuscany, Italy). *Canadian Mineralogist*, **49**, 623–638.

Orlandi, P., Biagioni, C., Bonaccorsi, E., Moëlo, Y. and Paar, W.H. (2012) Lead-antimony sulfosalts from Tuscany (Italy). XII. Boscardinite, $TlPb_3(Sb_7As_2)_{\Sigma 9}S_{18}$, a new mineral species from the Monte Arsiccio mine: occurrence and crystal structure. *Canadian Mineralogist*, **50**, 235–251.

Orlandi, P., Biagioni, C., Bonaccorsi, E., Moëlo, Y. and Paar, W.H. (2014) Bernarlottiite, IMA 2013-133. CNMNC Newsletter No. 20, June 2014, page 553; *Mineralogical Magazine*, **78**, 549–558.

Ribar, B., Nicca, C. and Nowacki, W. (1969) Dreidimensionale Verfeinerung der Kristallstruktur von Dufrénoysit, $Pb_8As_8S_{20}$. *Zeitschrift für Kristallographie*, **130**, 15–40.

Sheldrick, G.M. (2008) A short history of *SHELX*. *Acta Crystallographica*, **A64**, 112–122.

Topa, D. and Makovicky, E. (2016) Argentobaumhauerite: name, chemistry, crystal structure, comparison with baumhauerite, and position in the Lengenbach mineralization sequence. *Mineralogical Magazine*, **80**, 819–840.

Topa, D. and Makovicky, E. (2017) The crystal structure of veenite. *Mineralogical Magazine*, **81**, 355–368.

Topa, D., Makovicky, E., Tajedin, H., Putz, H. and Zagler, G. (2013) Barikaite, $Ag_3Pb_{10}(Sb_8As_{11})_{\Sigma 19}S_{40}$, a new member of the sartorite homologous series. *Mineralogical Magazine*, **77**, 3039–3046.

Topa, D., Keutsch, F.N., Makovicky, E., Kolitsch, U. and Paar, W. (2015) Polloneite, IMA 2014-093. CNMNC Newsletter No. 24, April 2015, page 249; *Mineralogical Magazine*, **79**, 247–251.

Wilson, A.J.C. (1992) *International Tables for Crystallography Volume C*. Kluwer, Dordrecht, The Netherlands.